Congenital Cataract-Causing Mutation G129C in γC-Crystallin Promotes the Accumulation of Two Distinct Unfolding Intermediates That Form Highly Toxic Aggregates

ARTICLE *in* JOURNAL OF MOLECULAR BIOLOGY · JULY 2015

Impact Factor: 4.33 · DOI: 10.1016/j.jmb.2015.07.001 · Source: PubMed

4 AUTHORS, INCLUDING:

Yi-Bo Xi

Tsinghua University

9 PUBLICATIONS **53** CITATIONS

SEE PROFILE

Xiangjun Chen

Tsinghua University

9 PUBLICATIONS **28** CITATIONS

SEE PROFILE

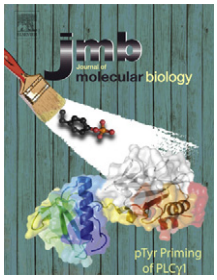

Congenital Cataract-Causing Mutation G129C in γC-Crystallin Promotes the Accumulation of Two Distinct Unfolding Intermediates That Form Highly Toxic Aggregates

Yi-Bo Xi[1,2,†], **Xiang-Jun Chen**[1,†], **Wei-Jie Zhao**[1,†] and **Yong-Bin Yan**[1]

*1 - **State Key Laboratory of Membrane Biology,** School of Life Sciences, Tsinghua University, Beijing 100084, China*
*2 - **Tsinghua–Peking Joint Center for Life Sciences,** School of Life Sciences, Tsinghua University, Beijing 100084, China*

***Correspondence to Yong-Bin Yan:** School of Life Sciences, Tsinghua University, Beijing 100084, China.*
ybyan@tsinghua.edu.cn
http://dx.doi.org/10.1016/j.jmb.2015.07.001
Edited by R. Wetzel

Abstract

Cataract is a lens opacification disease prevalent worldwide. Cataract-causing mutations in crystallins generally lead to the formation of light-scattering particles in the lens. However, it remains unclear for the detailed structural and pathological mechanisms of most mutations. In this study, we showed that the G129C mutation in γC-crystallin, which is associated with autosomal dominant congenital nuclear cataract, perturbed the unfolding process by promoting the accumulation of two distinct aggregation-prone intermediates under mild denaturing conditions. The abnormally accumulated intermediates escaped from the chaperone-like function of αA-crystallin during refolding. Molecular dynamics simulations indicated that the mutation altered domain pairing geometry and allowed the penetration of extra solvent molecules into the domain binding interface, thereby weakening domain binding energy. Under mild denaturation conditions, the increased domain movements may facilitate the formation of non-native oligomers via domain swapping, which further assembled into amyloid-like fibrils. The intermediate that appeared at 1.6 M guanidine hydrochloride was more compact and less aggregatory than the one populated at 0.9 M guanidine hydrochloride, which was caused by the increased solvation of acidic residues in the ion-pairing network via the competitive binding of guanidinium ions. More importantly, both the amyloid-like fibrils preformed *in vitro* and intracellular aggresomes formed by exogenously overexpressed mutant proteins significantly inhibited cell proliferation and induced cell death. The combined data from spectroscopic, structural and cellular studies strongly suggest that both the formation of light-scattering aggregates and the toxic effects of the aggregates may contribute to the onset and development of cataract.

Introduction

Non-native protein aggregation, a generic property of the marginally stable proteins, has been associated with a wide range of human disorders such as Alzheimer's disease, Huntington's disease, Parkinson's disease, amyotrophic lateral sclerosis and cataract [1–3]. The intracellular aggregates, aggresomes or inclusion bodies, are the off-pathway product of misfolded proteins, which are aggregation-prone folding intermediates with partially folded structures [4,5]. These misfolded proteins are originated from the erroneously folded nascent proteins, abnormal proteolytic polypeptides and denatured/damaged proteins by various physical and chemical stresses. Protein quality control system can help the cells to fight against these misfolded proteins and maintain protein homeostasis in the cells [6,7]. However, aggregates are formed when the misfolded proteins accumulate and exceed the critical concentration of protein aggregation. The intracellular aggregates may interfere with the cellular processes directly. For example, highly toxic molecular species formed during protein fibrillization are assumed to be the cause of neurodegenerative disorders [2]. As for cataract, the formation of light-scattering protein aggregates, no matter in amorphous or fibrillar morphologies, is thought to be the dominant cause of cataract via blocking the transmission of visible light through the lens [3].

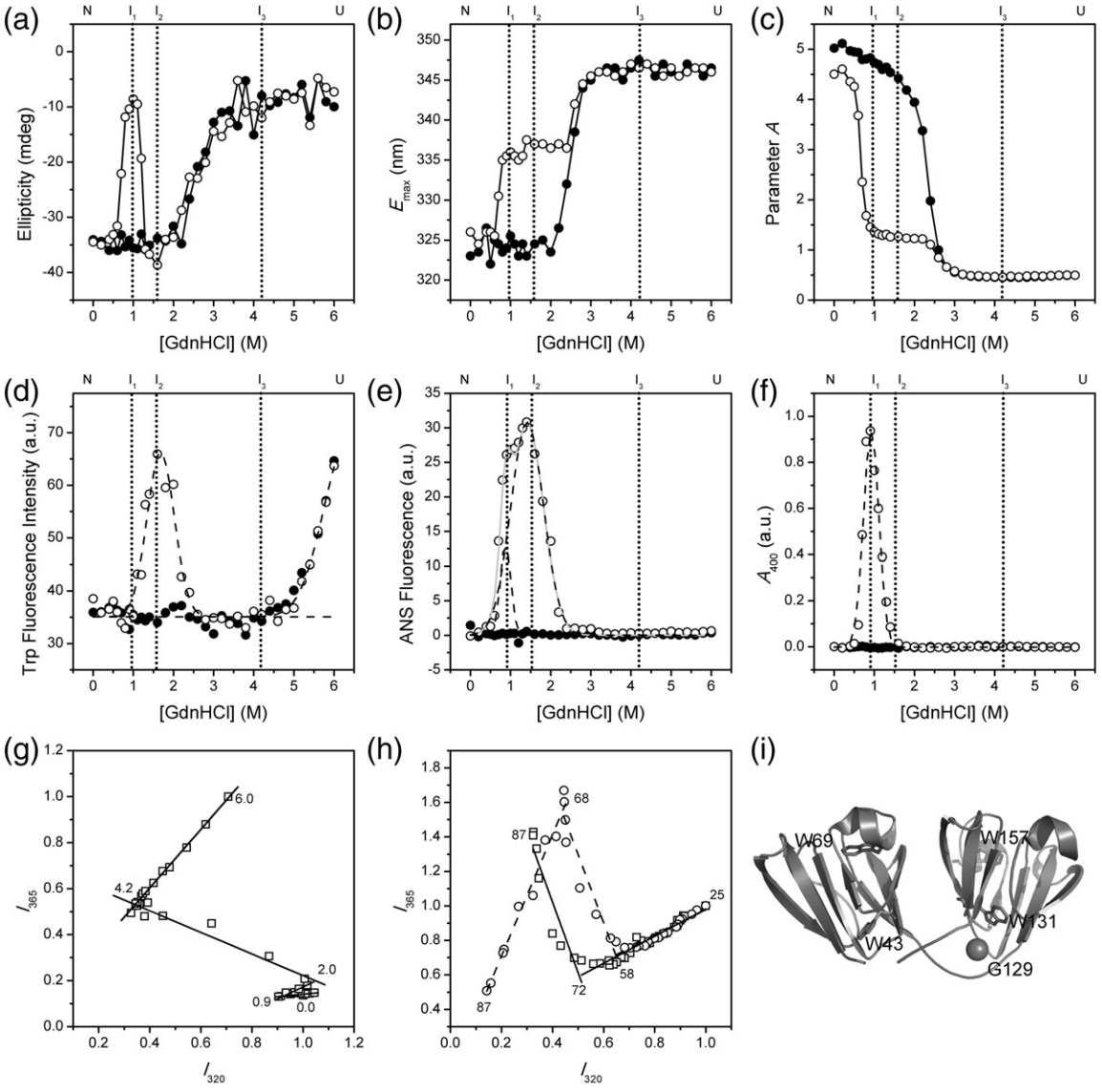

Fig. 1. Effect of the G129C mutation on the equilibrium unfolding of γC-crystallin. (a) GdnHCl-induced denaturation monitored by ellipticity at 222 nm. (b) GdnHCl-induced denaturation monitored by the maximum emission wavelength of Trp fluorescence (E_{max}). (c) GdnHCl-induced denaturation analyzed by Parameter *A* of Trp fluorescence. (d) Dependence of Trp fluorescence intensity on GdnHCl concentration. (e) Hydrophobic exposure of the proteins detected by ANS fluorescence. (f) Protein aggregation during GdnHCl-induced denaturation monitored by turbidity at 400 nm. (g) Phase diagram analysis of the Trp fluorescence spectra of the GdnHCl-denatured samples. (h) Phase diagram analysis of the Trp fluorescence spectra during thermal denaturation. (i) Crystal structure of mouse γC-crystallin (PDB ID: 2V2U) showing the positions of the mutation site and the four Trp fluorophores. The proteins were denatured by various concentrations of GdnHCl overnight (~12 h). The CD and fluorescence measurements were performed using the soluble fractions separated by centrifugation. In the phase diagram, the joint points are the GdnHCl concentrations where the intermediates accumulate. The phase diagram of thermal denaturation was achieved using the Trp fluorescence data reported previously [34]. From (a) to (f), the proximal positions of the intermediates are indicated by dotted lines, while the data of the WT and mutated proteins are presented in filled and open circles.

Cataract, which is the leading cause of human blindness worldwide, is the opacification of the lens resulting in visual impairment. Numerous factors have been associated with the onset of cataract in human beings [8–10], while genetic disorder is one of the most popular and well-defined causes in congenital cataract. Currently, about 45 genetic loci have been mapped to associate with isolated cataracts [10]. Among the >40 genes identified in non-syndromic Mendelian cataracts, lens crystallins are the major target for cataract mutations [10]. Crystallins are the predominant soluble proteins in

the cytoplasm of lens fiber cells. According to their elution volumes, vertebrate crystallins can be cataloged into three classes: α-, β- and γ-crystallins [11]. Among them, α-crystallins (αA and αB) belong to the small heat shock protein family with molecular chaperone-like function, while β/γ-crystallins are structural proteins sharing the same fold of four Greek-key motifs divided into two domains. High solubility and extreme longevity are the two most important properties of crystallins in maintaining the transparency of the lens. In cataractous lens, the deposition of various crystallins in the water-insoluble fractions is a general feature of various cataracts [3,12].

Many efforts have been devoted in recent years to elucidate the molecular mechanism of cataract caused by mutations or environmental factors [3,13–22]. The most widely understood mechanism is the disruption of crystallin solubility and/or stability directly by mutations/modifications or indirectly by changes in cellular homeostasis. It is worth noting that mutations in some of the crystallin genes have been associated with non-cataract abnormities such as neurodegenerative diseases, cardiomyopathy, tumorigenesis and retinal and vascular disorders [23–26]. Similar to proteins involved in neurodegenerative diseases, crystallins can also form amyloid-like fibrils under certain solution conditions [27–33]. However, the consequence of crystallin fibrillization in cataract formation, as well as in non-lens disorders, remains elusive since amorphous aggregates but not amyloid fibrils dominate the water-insoluble protein fractions isolated from cataractous lenses [3]. It has been hypothesized that the formation of amyloid-like fibrils has a possible action in cataract initiation [3], whereas the impact of amyloid-like fibrils on cellular processes remains unclear. In this research, this problem was addressed by investigating the cataract-causing mutation G129C in γC-crystallin.

The G129C mutation in γC-crystallin was identified recently in a Chinese family with autosomal dominant congenital nuclear cataract [34]. Previous mechanistic studies have revealed that the G129C mutation slightly impairs the tertiary structure, but it significantly decreases the thermal stability and accelerates the thermal aggregation of γC-crystallin. Importantly, injection of mutated human *CRYGC* genes into zebrafish embryos results in vacuole formation and incomplete denucleation of zebrafish lens [34]. This suggests that the mutated γC-crystallin interferes with the development of zebrafish lens. Herein we further showed that the mutation affected the unfolding pathway of γC-crystallin by stabilizing two distinct aggregation-prone intermediates. These two unfolding intermediates had different aggregatory properties, but both of them formed amyloid-like fibrils. The fibrils formed by the intermediates were toxic to the cells, suggesting that the accumulation of highly toxic fibril precursors or mature fibrils had a strong potential to impair the development of the lens and congenital cataract thereby.

Results

Effect of G129C mutation on the multi-state unfolding of γC-crystallin

Early studies have shown that the unfolding of γC-crystallin is a three-state process involving an intermediate state appeared between 2 and 3 M guanidine hydrochloride (GdnHCl) [35,36]. The structure of γC-crystallin is highly similar to γD-crystallin, which has been shown to fold via a multi-state pathway involving two kinetic intermediates [37,38]. Herein we further performed a comprehensive analysis to elucidate the impact of the G129C mutation on the unfolding pathway of γC-crystallin (Fig. 1). Most of the transition curves of the wild-type (WT) protein were similar to those reported previously [35,36]. Briefly, no significant changes were observed in the circular dichroism (CD) signal, E_{max} (maximum emission wavelength of intrinsic Trp fluorescence) and intensity of Trp fluorescence when GdnHCl concentration was below 2 M. Neither the 1-anilinonaphthalene-8-sulfonate (ANS) binding affinity nor the turbidity altered significantly along with the increase of GdnHCl concentration from 0 M to 6 M, suggesting that no hydrophobic sites were exposed and thus no off-pathway aggregates were formed during GdnHCl-induced denaturation of the WT γC-crystallin. Consistent with previous results [35], the change in Parameter *A* (Fig. 1c) could be best-fitted by a three-state model: native state (N) ↔ intermediate state (I) ↔ unfolded state (U). The free energy changes (ΔG_{H2O}) were 18 ± 6 and 43 ± 3 kJ/mol, while the denaturant susceptibility parameters (*m*) were 10 ± 4 and 19 ± 1 kJ/mol/mol for the transitions N ↔ I and I ↔ U, respectively. It is worth noting that the Trp fluorescence intensity increased abruptly when GdnHCl concentration was above 4.5 M. Similar phenomenon has also been observed in the unfolding of γD- and β-crystallins [37,39]. It has been proposed that the fluorescence of W69 and W157 is quenched in the native state of γD-crystallin, while that of W43 and W131 is not [37]. Considering the high conservation in the primary sequences and tertiary structures of γ-crystallins, the source of Trp fluorescence increase at high GdnHCl concentrations might also come from the native-state quenching of W69 and W157 in γC-crystallin. The increase in the Trp fluorescence intensity at high GdnHCl concentrations also suggested that the local structures around the Trp fluorophores were very resistant to denaturant.

The denaturation of the G129C mutant was the same as the WT protein at GdnHCl concentrations

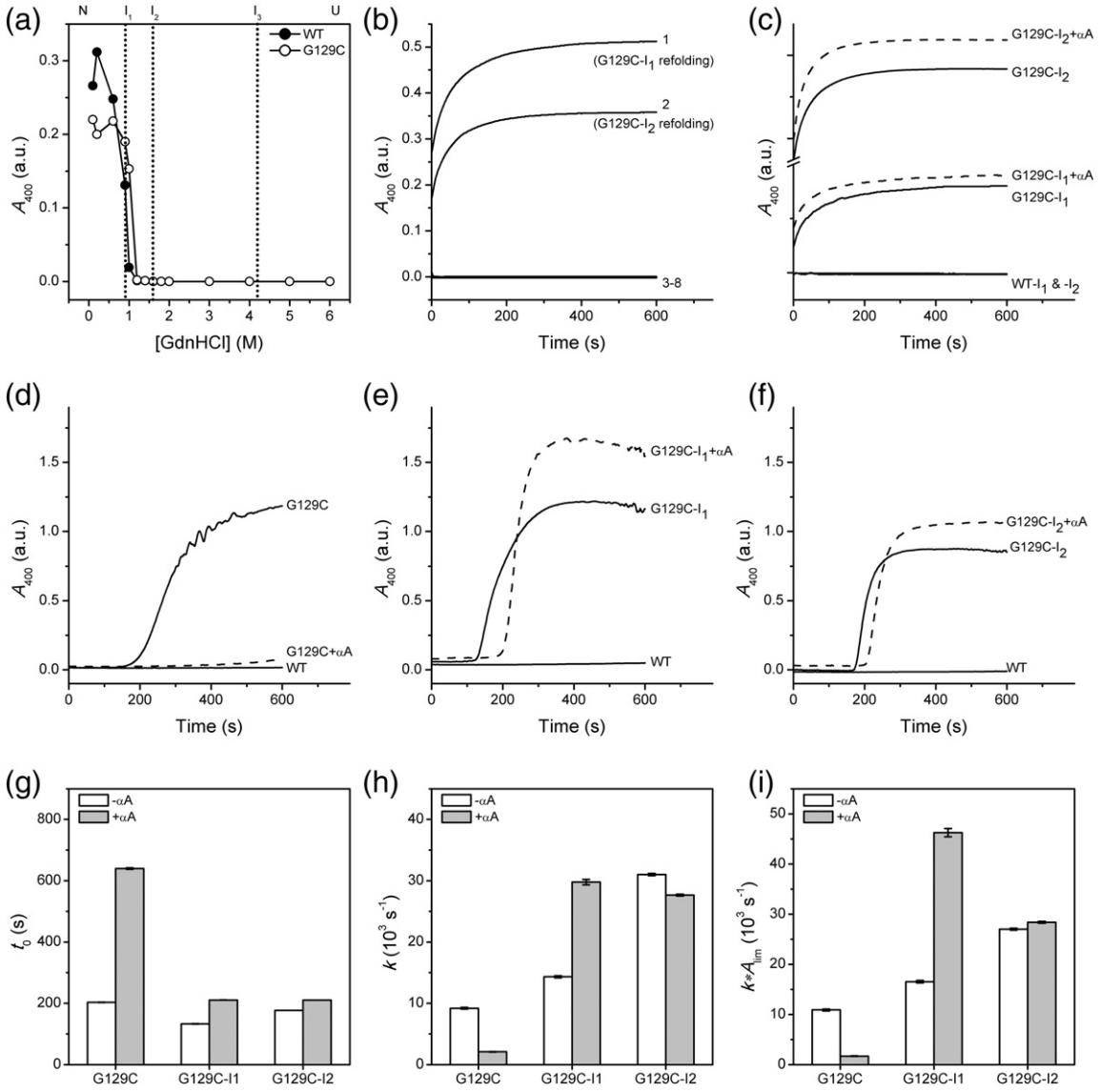

Fig. 2. Properties of the two distinct unfolding intermediates of the G129C mutant. (a) Protein aggregation during the equilibrium refolding of 6 M GdnHCl-denatured WT and mutated γC-crystallins. The proteins were fully denatured in PBS containing 6 M GdnHCl at ambient temperature overnight. The denatured proteins were diluted into PBS containing various concentrations of GdnHCl and the turbidity at 400 nm was measured after a 12-h incubation of the samples. (b) Aggregation during the kinetic refolding and unfolding of the intermediates I_1 at 0.9 M GdnHCl and I_2 at 1.6 M GdnHCl. Kinetic refolding and unfolding were initiated by diluting the intermediates into PBS in the absence or presence of 8 M GdnHCl, respectively. Lines 1 and 2 are the aggregation during the refolding of G129C-I_1 and G129C-I_2, respectively. Lines 3–8, which are indistinguishable, are the refolding of WT-I_1 and WT-I_2 and the unfolding of the four intermediates. (c) Effect of αA-crystallin on the aggregation during the kinetic refolding of the intermediates I_1 and I_2. (d) Effect of αA-crystallin on the thermal aggregation of the native proteins at 70 °C. (e) Effect of αA-crystallin on the thermal aggregation of I_1 at 70 °C. (f) Effect of αA-crystallin on the thermal aggregation of I_2 at 70 °C. (g) Effect of αA-crystallin on the lag time t_0. (h) Effect of αA-crystallin on the aggregation rate k. (i) Effect of αA-crystallin on the initial velocity of thermal aggregation ($k \times A_{lim}$). The kinetic parameters of γC-crystallin thermal aggregation were obtained by fitting the raw data in (d–f) by Eq. (1).

above 2.8 M. However, quite different behavior was observed for all the transition curves when denatured at low GdnHCl concentrations. There was a long platform between 0.8 M and 2.4 M GdnHCl in the changes of E_{max} and Parameter A, indicating that there might exist more than one intermediate state at low GdnHCl concentrations. In supporting this proposal, the changes in ANS were best-fitted by

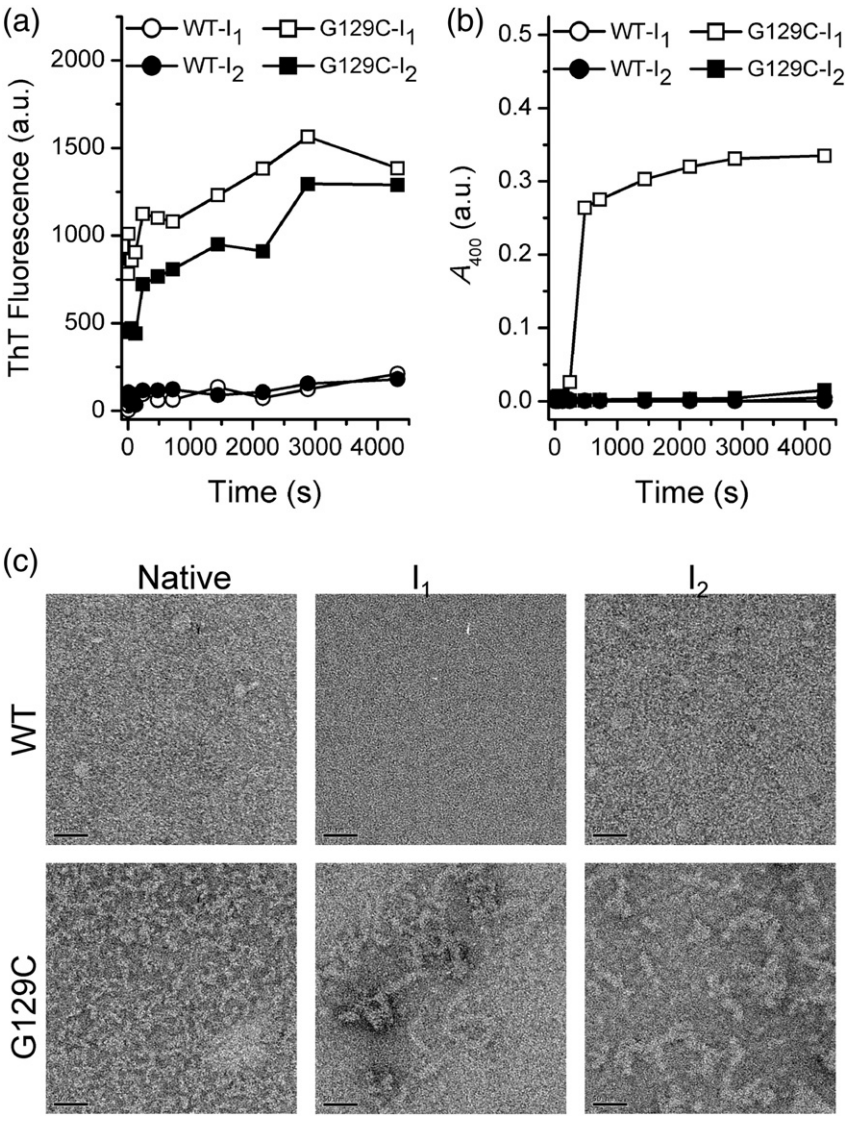

Fig. 3. The G129C mutant of γC-crystallin forms amyloid-like fibrils. (a) Fibrillization of the intermediate states detected by ThT fluorescence. (b) Turbidity of the incubated samples. (c) Negatively stained transmission EM pictures of the samples incubated for 72 h. Protein fibrillization was carried out by incubating 5 mg/ml proteins at 37 °C. The ThT, turbidity and EM measurements were performed using 0.2 mg/ml diluted samples. The scale bar represents to 50 nm.

two peaks rather than by one peak (Fig. 1e), suggesting that there were two intermediate states populated at around 0.9 M (I_1) and 1.6 M GdnHCl (I_2). These two intermediates had distinct properties although both of them had large hydrophobic exposure. In detail, I_1 was more prone to aggregation than I_2 as evidenced by the dramatic increase in turbidity around 0.9 M GdnHCl (Fig. 1f). Due to the appearance of aggregates, the ellipticity had an abrupt decrease at around 0.9 M GdnHCl (Fig. 1a), which was caused by the removal of insoluble fractions by centrifugation before CD experiments. The intermediate I_2 had similar content of regular secondary structures to the native state (Fig. 1a) and almost identical Trp fluorescence intensity with the fully unfolded state (Fig. 1d). Nonetheless, the most striking alteration of these two intermediates caused by the mutation was the behavior of the four Trp fluorophores, which are located around the hydrophobic core of the domains (Fig. 1i).

Fitting the unfolding data of the WT γC-crystallin indicated that there was only one populated intermediate. To explore whether the G129C mutation altered the unfolding pathway of γC-crystallin, we constructed a phase diagram, a sensitive tool to detect hidden intermediates, and showed it in Fig. 1g. In the phase diagram, a straight line represents a two-state transition and the joint position of straight

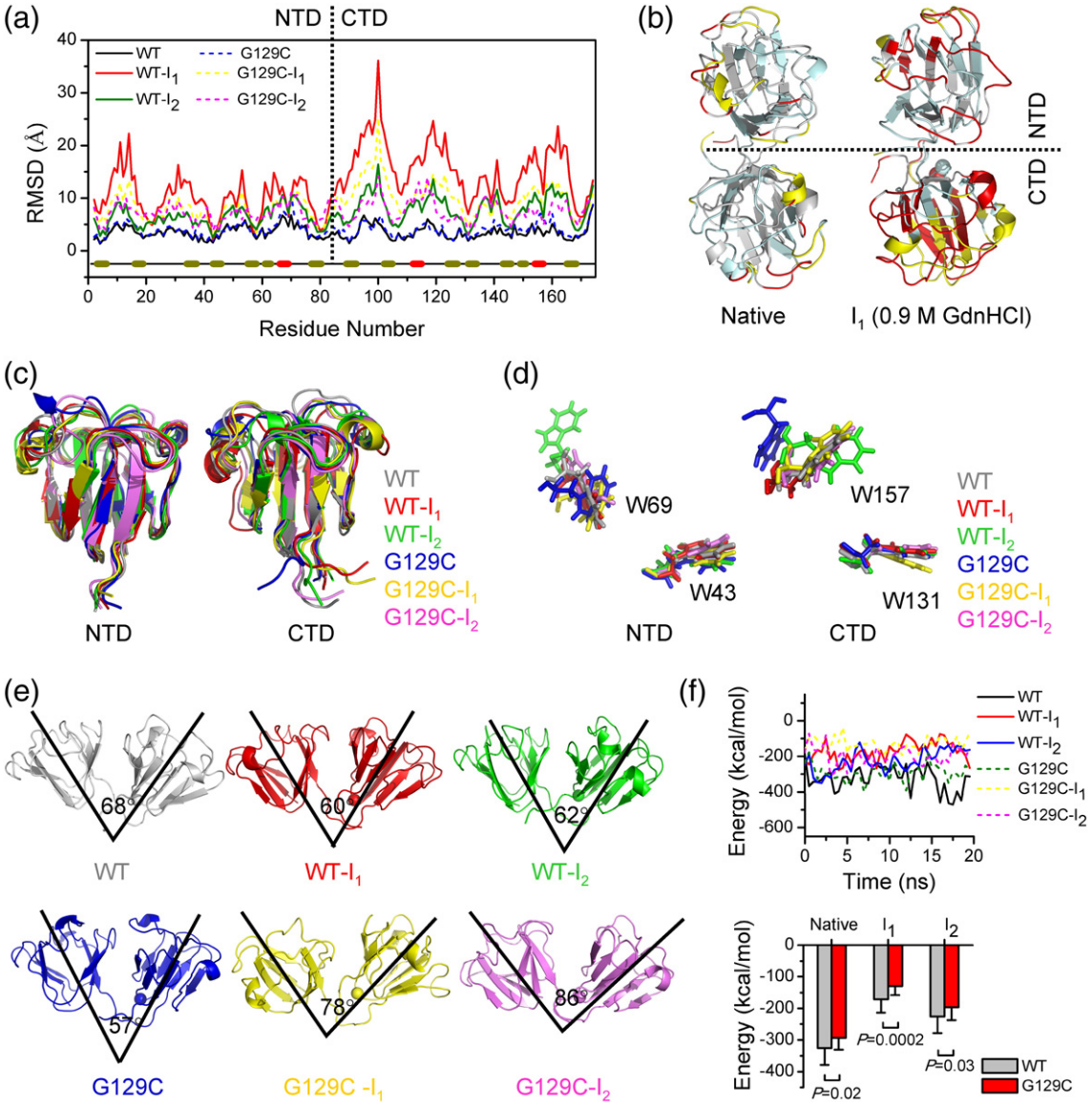

Fig. 4. Structural variations induced by the G129C mutation and low concentrations of GdnHCl studied by MD simulations. (a) Structural variations of the proteins during simulations. The secondary structure elements are shown below the RMSD values. Black, random coils; dark yellow, β-strands; red, helices. (b) Positions of the highly flexible regions in the native proteins (RMSD > 5 Å) and the intermediate I_1 (RMSD > 10 Å). The WT and G129C γC-crystallins are rendered in gray and pale cyan, respectively. The flexible regions are highlighted in red and yellow for the WT protein and G129C mutant, respectively. (c) Structural alignments of NTD and CTD. (d) Changes in the positions of the Trp fluorophores in the aligned NTD and CTD. (e) Changes in domain pairing geometry by the G129C mutation and low concentrations of GdnHCl. (f) Domain binding energies. The upper panel shows the fluctuations of binding energies during MD simulations, and the lower panel shows the average values of domain binding energies.

lines means the intermediate state [40]. The phase diagram clearly showed that there were three intermediates appeared at around 0.9 M (I_1), 2.0 M (I_2) and 4.2 M GdnHCl (I_3), which were identical with those identified in the denaturation of the G129C mutant. Particularly, the existence of the aggregation-prone intermediate I_1, which was invisible by normal analytical methods, was verified the appearance of aggregates at GdnHCl concentrations below 1.0 M GdnHCl during the equilibrium refolding of the denatured γC-crystallin (Fig. 2a). The folding mechanism of γC-crystallin characterized herein is similar to that of γD-crystallin [38] except for the existence of I_3. Thus, the G129C mutation did not alter the folding mechanism of γC-crystallin, but it modified the properties of the native state and intermediates I_1 and I_2. The effect of the

G129C mutation on the GdnHCl-induced denaturation was different from that on the thermal denaturation of γC-crystallin. Phase diagram analysis of the Trp fluorescence data during thermal denaturation presented in our previous paper [34] indicated that the mutation induced an additional aggregation-prone intermediate state at around 68 °C (Fig. 1h). The difference may be caused by the different nature of denaturation induced by heat or chemical denaturants.

The aggregation-prone intermediates of the G129C mutant escape from the chaperone function of αA-crystallin

The results in Fig. 1 indicated that the G129C mutation promoted off-pathway aggregation during γC-crystallin denaturation. However, equilibrium refolding studies showed that the WT γC-crystallin was also prone to get trapped into the aggregation pathway, and γC-crystallin refolding was not significantly affected by the mutation (Fig. 2a). Dissimilarity in the unfolding and refolding pathways has also been observed in γD- and β-crystallins [38,39]. When the WT protein was denatured by 0.9 M or 1.6 M GdnHCl, the partially denatured proteins could successfully refold via fast dilution (Fig. 2b). However, the partially denatured G129C failed to refold and aggregated immediately after dilution. As the control, both proteins could be fully denatured and solubilized by 8 M GdnHCl. The aggregation of the G129C intermediates I_1 and I_2 could not be inhibited by the addition of αA-crystallin in the refolding buffer (Fig. 2c). Furthermore, the thermal aggregation of the native G129C mutant could be efficiently inhibited by the existence of αA-crystallin (Fig. 2d), but it could hardly for the intermediates I_1 and I_2 (Fig. 2e and f). Fitting of the turbidity data using Eq. (1) indicated that although the lag time t_0 was slightly elongated, the aggregation rate k and the initial aggregation velocity $k \times A_{lim}$ were either accelerated (for I_1) or unaffected (for I_2) by αA-crystallin during the thermal aggregation of the G129C intermediates (Fig. 2g–i). Thus, the partially denatured G129C intermediates could successfully escape from the quality control action of αA-crystallin although the aggregation of the native state of the G129C mutant could be rescued by αA-crystallin. Similarly, it has been found recently that γD-crystallin mutants in mouse models have low affinity to α-crystallin [41].

The unfolding intermediates of G129C mutant form amyloid-like fibrils

After long-term incubation, both I_1 and I_2 of G129C could form aggregates. To investigate the nature of these aggregates, we performed time-course study by monitoring the thioflavin T (ThT) fluorescence and turbidity during the incubation of the WT or G129C proteins in buffers containing 0.9 M or 1.6 M GdnHCl at physiological temperature. The changes of the WT γC-crystallin were neglectable, while both G129C-I_1 and G129C-I_2 formed ThT-positive aggregates (Fig. 3a). Consistent with the equilibrium unfolding data shown in Fig. 1f, G129C-I_1 but not G129C-I_2 produced considerable amounts of aggregates with large light scattering (Fig. 3b). The morphology of the aggregates was visualized by negatively stained transmission electron microscope (EM). Both G129C-I_1 and G129C-I_2 formed fibrillar aggregates with similar width of about 15 nm, while the native G129C protein formed thinner and smaller fibrillar structures (Fig. 3c). Thus, denaturation by 0.9 M GdnHCl provided G129C the optimal condition of fibrillization.

Structural insight into the effect of G129C mutation on γC-crystallin stability and folding

Since the high-resolution structure of human γC-crystallin has not been resolved yet, the starting structures of the WT human γC-crystallin and the G129C mutant were constructed by homology modeling using the crystal structures of human γD-crystallin (PDB ID: 1HK0) [42] and mouse γC-crystallin (PDB ID: 2V2U) [43]. Molecular dynamics (MD) simulations were performed for the proteins in the presence or absence of low concentrations of GdnHCl to mimic the intermediate states of I_1 and I_2 identified above (Supplementary Fig. 1). The RMSD values per residues of all simulations followed a similar pattern (Fig. 4a), and the most flexible regions were located at the loops and linker region (Fig. 4b). Interestingly, the proteins in the existence of 0.9 M GdnHCl but not 1.6 M GdnHCl had the largest structural variations, while the variations of the WT protein were ever larger than the mutant. For the native proteins, no significant difference was observed for the flexibility between the N-terminal domain (NTD) and the C-terminal domain (CTD). However, the existence of 0.9 or 1.6 M GdnHCl increased the flexibility of CTD much larger than that of NTD, particularly for the outward β-strands (Fig. 4b). Alignment of the isolated NTD or CTD indicated that the core Greek-key motifs were well maintained for all simulating conditions (Fig. 4c). The maintenance of the core structure observed by MD simulations is consistent with the little change in secondary structures when denatured by GdnHCl lower than 2 M (Fig. 1a). The Trp fluorophores could be partially affected by low concentrations of GdnHCl (Fig. 1b–d and g). Consistently, MD simulations indicated that, among the four Trp fluorophores, the positions of W43 and W131 were well retained although the mutation site of G129C is adjacent to W131. On the contrary, the orientations of W69 and W157 varied greatly by the mutation and the addition of GdnHCl (Fig. 4d). Mutational and spectroscopic experiments have

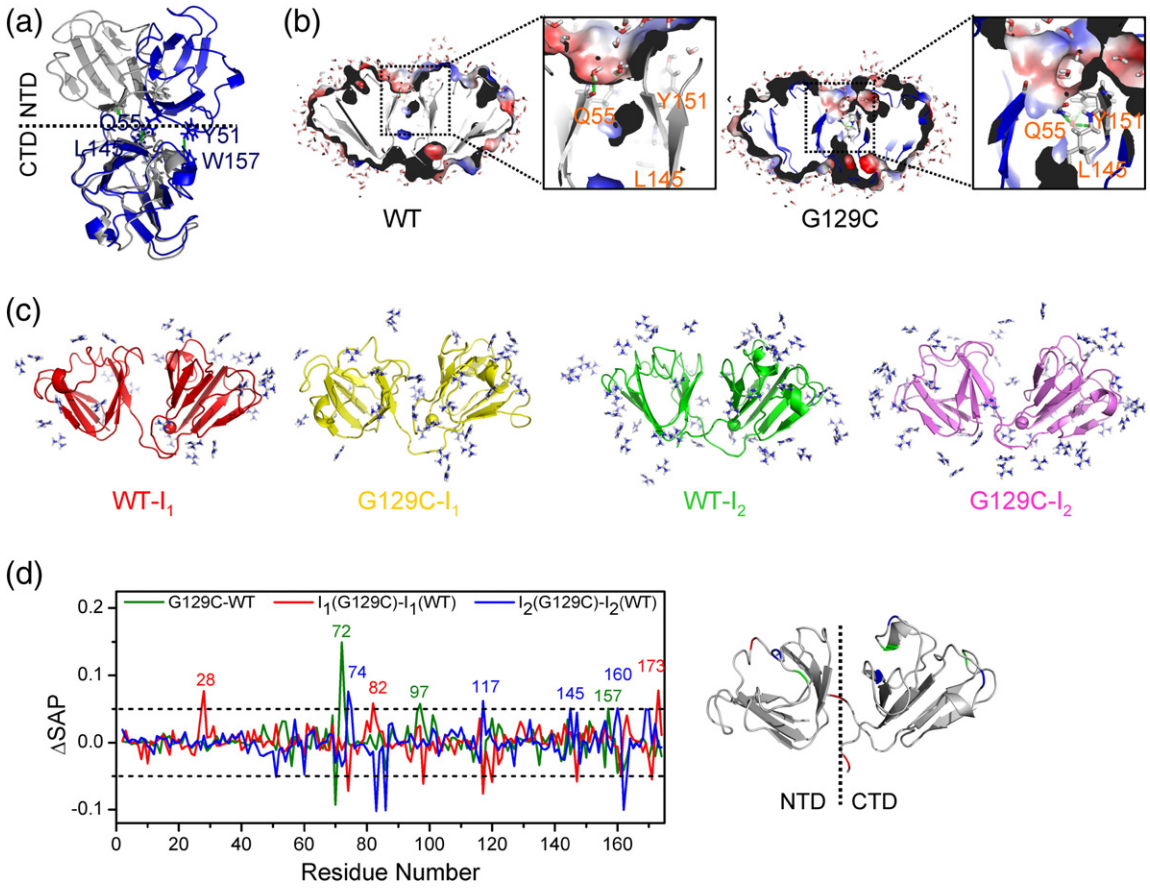

Fig. 5. Solvation of the WT and G129C γC-crystallins by MD simulations. (a) Changes in domain interaction interface by the G129C mutation. Two extra backbone H-bonds are formed in the domain interface of G129C. The structures of the WT and mutated γC-crystallin are aligned by CTD. (b) Penetration of an extra water molecule in the domain interaction interface of G129C. The penetrated water molecule forms H-bonds with adjacent residues. The structures were shown by an 8-Å clip. (c) Binding of the proteins with guanidinium ions. The guanidinium ions within 3 Å from the proteins are shown in the ball-and-stick model. (d) Difference in the SAP scores between the WT and mutated proteins. Amino acid residues with ΔSAP > 0.05 are labeled and distinguished by different colors for each state. The right panel shows the positions of residues with ΔSAP > 0.05 in the three-dimensional structure of γC-crystallin. Green, red and blue are sites in the native state, I_1 and I_2, respectively.

revealed that W69 and W157 are the source of native-state quenching of human γD-crystallin [37,44]. Thus, the results in Fig. 4d suggest that the microenvironmental changes around W69 and W157 by the mutation and/or GdnHCl were more likely to contribute to the fluorescent perturbations during the denaturation of the WT and mutated γC-crystallin (Fig. 1c and g).

Although Fig. 4a–d showed that there were structural changes induced by the G129C mutation and GdnHCl, we failed to identify the structural origin of the aggregation-prone property of G129C intermediates from the view of core structural fold or flexibility of the loops. A close inspection of the tertiary structures indicated that the domain pairing geometry changed little for the WT protein when denatured by low concentrations of GdnHCl (Fig. 4e). However, the angle between the contacted two domains became increasingly larger when G129C was denatured by GdnHCl. A quantitative determination of the pairing of the two domains was achieved by calculating the interdomain interface areas using PDBePISA [45]. The interface areas were 565.9 $Å^2$, 580.7 $Å^2$, 674.6 $Å^2$, 695.8 $Å^2$, 581.4 $Å^2$ and 446.3 $Å^2$ for WT, WT-I_1, WT-I_2, G129C, G129C-I_1 and G129C-I_2, respectively. Thus, the interdomain interface of G129C was more easily affected by denaturant than that of the WT γC-crystallin. Although the G129C mutation increased the interdomain interface area of γC-crystallin, the binding energy between NTD and CTD was slightly decreased by the mutation (Fig. 4f). The divergence between the interface area and binding energy results may be caused by the different nature of the methods. In this case, the larger interface area but slightly smaller binding energy

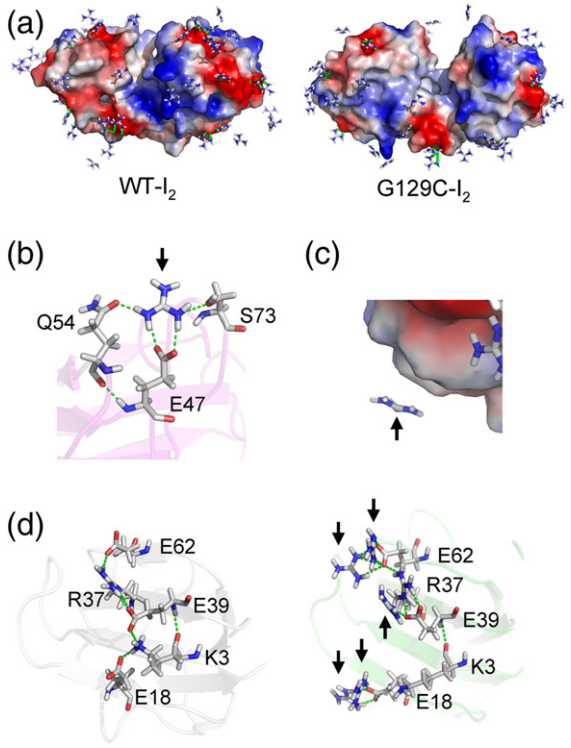

Fig. 6. Guanidinium ions prefer to bind with the negatively charged or polar groups and compete with the positively charged side chains in ion pairs. (a) The guanidinium ions prefer to bind with the negatively charged clusters on protein surfaces. The guanidinium ions are shown in the ball-and-stick model. Red, blue and white surfaces of the proteins represent negatively charged, positively charged and hydrophobic surface potentials. (b) Guanidinium ions prefer to bind with the negatively charged or polar groups. One guanidinium ion can form H-bonds with more than one residue. (c) Guanidinium ions can access, though only for limited cases, the hydrophobic surfaces with an orientation parallel with the surface. (d) Competition of guanidinium ions with the positively charged side chains in ion pairs. Left: ion-pairing network in the native state of WT γC-crystallin, right: disruption of the ion-pairing network by competition of guanidinium ions in WT-I_2. For clarity, the guanidinium ions are indicated by black arrows.

implied that the mutation induced a non-native and loosely packed domain interface. It is worth noting that the time-course study showed that the binding energies of all proteins had considerable fluctuations around the average value, which covered up the difference between the WT and mutated proteins. The high level of fluctuations over the course of simulations also suggested that the domain interface of γC-crystallin might be intrinsically dynamic.

The native structure of G129C had a smaller angle of domain pairing and a larger domain interface area when compared with the WT protein. Alignment based on CTD showed that the G129C mutation resulted in an about 60° twist of NTD accompanied with the change of the binding interface (Fig. 5a). Particularly, two new H-bonds were formed between NTD and CTD residues: backbone NH of W157 to backbone C = O of Y51 and backbone NH of L145 to side chain C = O of Q55. It is possible that the new structural constraints altered the packing of the two domains and therefore different binding interface. More importantly, analyzing the water molecules within 3 Å of the protein indicated that the domain binding interface of the WT γC-crystallin is dry and lack of interior water molecules, while water can penetrate into the binding interface of G129C and stabilizes the new interface in the mutant via interacting with Q55, L145 and Y151 (Fig. 5b). In supporting this observation, we have shown previously that the size-exclusion chromatography profile of G129C contained a much wider peak eluted at an earlier volume than the WT protein [34]. Combined with the results herein, it is safe to conclude that the mutation altered the hydrodynamic radius/molecule shape of γC-crystallin. This might be the reason why the mutant had a larger interdomain interface area but smaller binding energy (Fig. 4f). The modified domain binding interface facilitated the solvent molecules to penetrate in and thereby weakened the pairing of the two domains when denatured by low concentrations of GdnHCl. Consistently, guanidinium ions were more easily to attack the interdomain regions of G129C when compared with the WT protein. In detail, guanidinium ions were unable to penetrate in the interdomain interfaces of WT-I_1 and WT-I_2, while 0–2 guanidinium ions could be found in interfaces of G129C-I_1 and G129C-I_2 over the course of simulation (Fig. 5c).

To explore why G129C-I_1 had the highest aggregatory propensity, we calculated and compared the spatial aggregation propensity (SAP) values. SAP, which is calculated from the dynamically exposed hydrophobicity of a residue on protein surface, is a measure of aggregation-prone property of each residue [46]. A higher value indicates a stronger aggregation-prone property. Compared with the native state, both the WT and G129C γD-crystallins had residues with high ΔSAP values when simulated under denaturing conditions (Supplementary Fig. 2), while G129C had more. Moreover, all states of G129C had extra aggregation-prone residues when compared with the corresponding states of the WT protein, but all differed in the positions of the sites with high ΔSAP values. Most of the residues with high ΔSAP values are located at CTD. Actually, CTD was more hydrophobic in the G129C mutant than in the WT protein, while the difference in NTD was minor. Previously, it has been shown that CTD is the site of nucleation and fibrillization of human γD-crystallin, while NTD is disordered in the amyloid-like fibrils [32,47]. The relatively higher hydrophobicity of CTD might contribute to the aggregation-prone property of the G129C mutant of human γC-crystallin. However, we could not assign whether the dissimilarity in the high ΔSAP sites was responsible to the

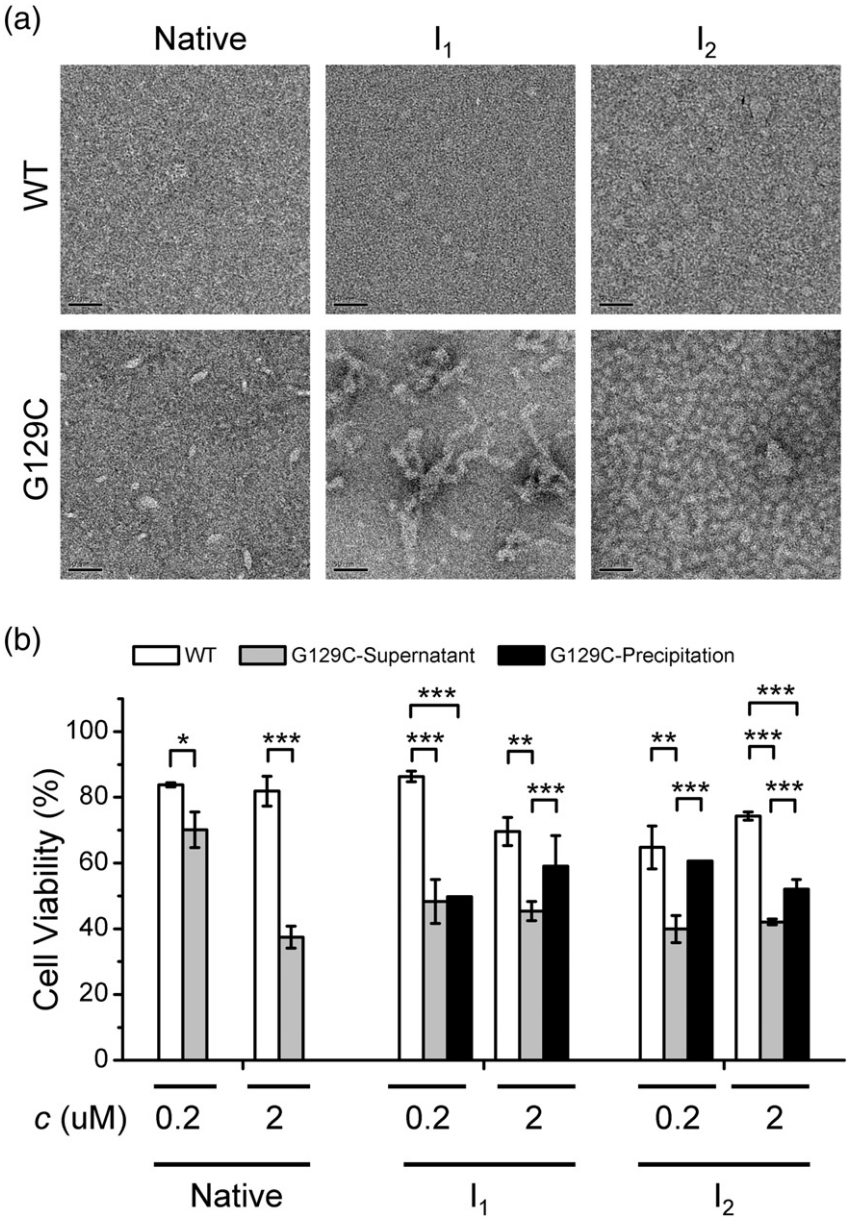

Fig. 7. The preformed γC-crystallin aggregates are toxic. (a) Negatively stained EM pictures of the soluble fractions of the protein solutions after a 72-h incubation. (b) Effect of the protein aggregates on cell viability. The preformed protein aggregates were prepared by incubating 5 mg/ml proteins at 37 °C for 72 h. Then the protein solutions were centrifuged to separate the large (precipitation fraction) and small (supernatant fraction) aggregates. No precipitation fractions were available for the WT proteins and the native G129C mutant. The HeLa cells were treated by 0.2 or 2 μM protein solutions/aggregates for 48 h and then cell viability was assayed using CCK-8 kit. *$P < 0.05$, **$P < 0.01$ and ***$P < 0.001$.

difference in the aggregation rate among the native G129C, G129C-I_1 and G129C-I_2.

The biophysical basis of protein denaturation by denaturant remains to be elucidated despite many years of research. Our MD simulation results showed that guanidinium ions preferred to interact with the charged and polar areas than the hydrophobic areas on protein surface (Fig. 6a). This is consistent with the fact that GdnHCl is an ionic denaturant under physiological conditions. At least under low GdnHCl concentration conditions, the guanidinium ions preferred to form H-bonds with amino acid side chains containing carboxyl (Asp and Glu), carbonyl (Gln and Asn) and hydroxyl (Tyr, Ser and Thr) groups. One guanidinium ion could bind more than one group (Fig. 6b), implying that guanidinium ions had the possibility to stabilize non-native, side-chain interactions. Though there

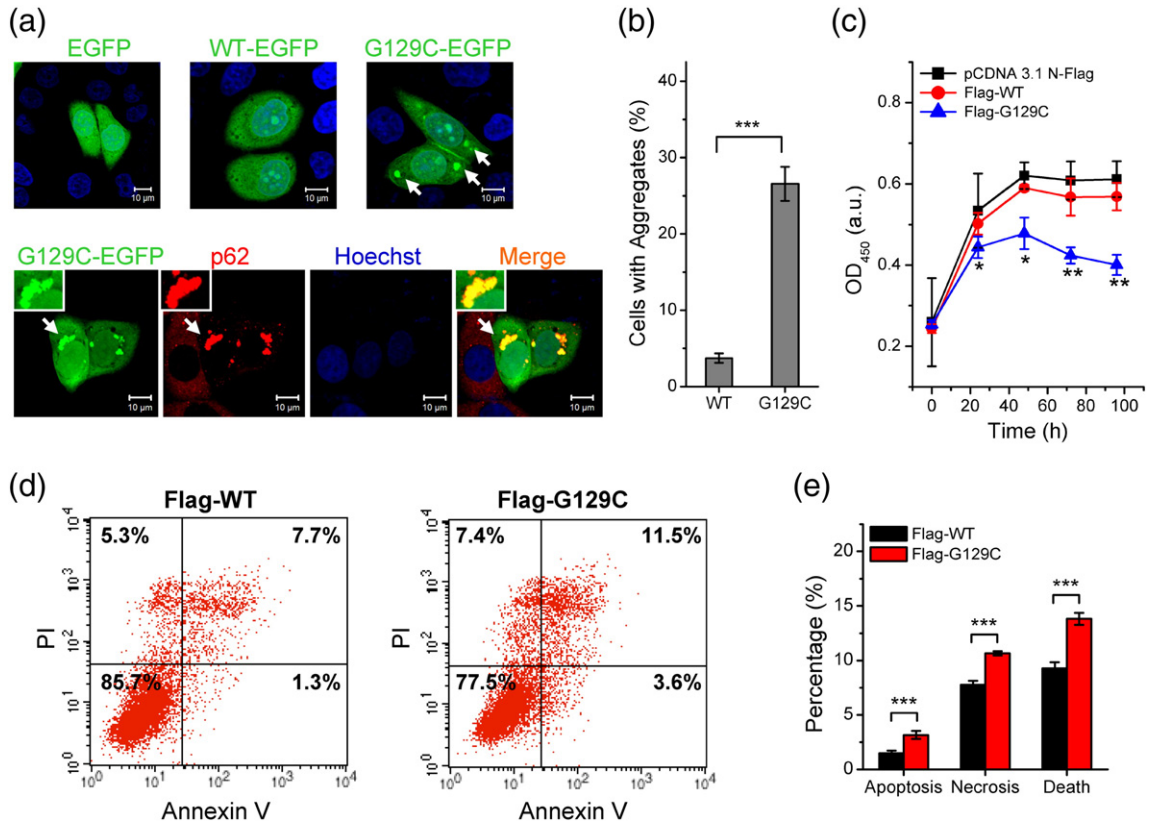

Fig. 8. The exogenously expressed G129C mutant of γC-crystallin inhibits cell proliferation and induces cell death. (a) The exogenously expressed G129C mutant of γC-crystallin forms p62-positive aggresomes in HeLa cells. Typical aggresomes are indicated by white arrows. (b) Quantitative analysis of aggresome formation in the HeLa cells. (c) The exogenously expressed G129C mutant inhibited HeLa cell proliferation. HeLa cells transfected with pcDNA 3.1 N-Flag plasmids were used as the negative control. (d) Representative flow cytometry profiles of cell death probed by annexin V binding (horizontal) and PI exclusion (vertical). (e) Percentages of apoptotic and necrotic cells. The percentages of dead cells were the sum of apoptotic and necrotic cells. $^{*}P < 0.05$, $^{**}P < 0.01$ and $^{***}P < 0.001$.

were not many cases, guanidinium ions could also cover the hydrophobic surfaces (Fig. 6c). The guanidine plane was nearly parallel with the hydrophobic surface. Our observation is consistent with the previous MD simulation study using modeled polymer surfaces [48]. Another structural impairment induced by guanidinium ions was to compete with the positively charged residues in ion pairs to form H-bonds with the negatively charged groups (Fig. 6d). One ion pair may contribute several kilocalories per mole to the stability of proteins [49]. Thus, once the surface charge clusters were altered by mutations, the behavior of protein denaturation could be affected and the properties of the intermediate states could also be modified.

The G129C aggregates are toxic to the cells

To investigate the pathological implications of G129C aggregation, we formed fibrillar aggregates by incubating 5 mg/ml proteins in the presence of 0.9 M or 1.6 M GdnHCl for 72 h. The supernatant and precipitation fractions were separated by centrifugation to compare the effects of small and large aggregates. The morphology of the supernatant fractions was visualized by EM (Fig. 7a). Unlike the results shown in Fig. 3a, the supernatant fractions of the G129C incubated in the absence of GdnHCl contained limited number of small aggregates or soluble oligomers. G129C-I_1 contained considerable amounts of short fibrils, while G129C-I_2 had plenty of short rod-like aggregates. Despite the difference in morphology, all G129C samples had significant toxic effect on HeLa cells (Fig. 7b). At low protein concentrations, the toxic effect of native G129C was minor and much smaller than those of G129C-I_1 and G129C-I_2. At high protein concentrations, similar toxic effects were observed for all aggregates no matter which states they were formed from. Generally, the toxic effects of the precipitation fractions were weaker than the supernatant fractions. Notably, the WT protein incubated in the presence of GdnHCl also exhibited minor toxic effect by decreasing cell viability

about 10%, which might be caused by those high concentrations of WT γC-crystallin that could also form small oligomers/aggregates after long-term incubation under mild denaturing conditions.

The effect of overexpressed G129C mutant on the growth and survival of HeLa cells was studied by transfecting HeLa cells with WT or mutated *CRYGC* genes. The exogenously expressed WT γC-crystallin showed disperse distribution in both cytoplasm and nucleus of the HeLa cells, which had a similar pattern to the EGFP control (Fig. 8a). The G129C mutant was prone to concentrate in micrometer-sized cytoplasmic foci, which were perfectly colocalized with the aggresome marker p62 (Fig. 8a and b). The exogenously expressed WT γC-crystallin did not affect the growth of the HeLa cells, whereas G129C significantly inhibited cell proliferation (Fig. 8c). The effect of exogenously expressed γC-crystallins on cell death was analyzed by bivariate flow cytometry using propidium iodide (PI) and annexin V double staining (Fig. 8d). Compared to cells overexpressing WT γC-crystallin, cells overexpressing G129C had a significant increase in the percentages of apoptotic and necrotic cells (Fig. 8e). Thus, the results in Figs. 7 and 8 suggested that the aggregates of G129C, no matter whether they were formed inside or outside the cells, had a pronounced effect on cell proliferation and cell death.

Discussion

Cataract-causing mutations usually lead to crystallin aggregation and/or destabilization but may do so via quite dissimilar mechanisms [50]. Herein we showed that the G129C mutant had a similar multi-state unfolding pathway to the WT γC-crystallin protein. The major deleterious effect of the G129C mutation was to facilitate the accumulation of aggregation-prone intermediates under mild denaturing conditions (Fig. 1). The exposure of extra hydrophobic sites is one of the driving forces of protein aggregation [1,2,51]. We did observe difference in hydrophobic exposure between the WT and mutated proteins. However, the overall hydrophobicity of the mutant was similar to the WT protein under all denaturing conditions during MD simulations (Fig. 5d). Thus, the increased hydrophobic exposure of the mutant during denaturation was more likely to be caused by the formation of off-pathway oligomers with high ANS-binding affinity [52]. MD simulations indicated that the G129C mutation might alter the domain interaction interface and thereby the pairing geometry of the two domains (Fig. 4). The modified domain interface was more readily penetrated by solvent molecules and weakened by denaturants (Fig. 5). Under mild denaturing conditions, the increased domain movements might facilitate the formation of non-native oligomers via domain swapping, which has been proposed to be one of the mechanism of γD-crystallin aggregation [47]. The proposal of abnormal intermolecular pairing between NTD and CTD during γ-crystallin aggregation is also supported by the observation that isolated domains have lower fibrillization propensity than the full-length γD-crystallin [29]. Unexpectedly, we found that, in the presence of 0.9 M GdnHCl, the WT protein exhibited the largest structural variations (Fig. 4a). However, the large structural variations of WT-I_1 did not result in extra hydrophobic exposure sites and thus WT-I_1 had low aggregatory potency (Supplementary Fig. 2). This observation is consistent with the proposal that, at least in some cases, the structural stability and aggregatory propensity of proteins are separated [53].

Interestingly, we identified two distinct aggregation-prone intermediates but dissimilar biophysical properties (Fig. 1). G129C-I_1 had an extremely high aggregation propensity and resulted in fast deposition of large aggregates, while G129C-I_2 had a slow oligomerization process followed by the formation of fibrillar structures after long-term incubation. Despite the difference in the rate of aggregation, these two intermediates harbored similar property of escaping from the chaperone-like function of α-crystallin (Fig. 2) and similar toxicity to the cells (Fig. 7). Though G129C-I_1 and G129C-I_2 had dissimilar exposed hydrophobic sites when compared with the WT protein under the same denaturing conditions, it is difficult to conclude whether hydrophobic attractions were responsible to the difference observed in aggregation propensity (Fig. 5d). Surprisingly, MD simulations indicated that WT-I_2 and G129C-I_2 had smaller structural variations and tighter domain pairing than WT-I_1 and G129C-I_1, respectively (Fig. 4). This implied that some of the native structures were destroyed by 0.9 M GdnHCl, while 1.6 M GdnHCl recovered part of the native structures or induced new stabilizing structures. The protein stabilization and regular secondary structure induction effects of low concentrations of denaturants have also been observed in several other proteins [54–56]. Our MD simulations indicated that the proteins bound more guanidinium ions when denatured in 1.6 M than in 0.9 M GdnHCl solutions (Figs. 5 and 6). The increased solvation may contribute to the stabilization of the proteins in 1.6 M GdnHCl solutions. Another possible mechanism is that some of the ion pairs were energetically unfavored due to the opposing effect of stabilization by ion pair and destabilization by desolvation. In 1.6 M GdnHCl solutions, guanidinium ions released and solvated more acidic residues from ion pairs and thus an overall stabilizing effect could be observed when compared with proteins in 0.9 M GdnHCl solutions.

Cataract is a disease that is directly linked to the aggregation of crystallins, the predominant fraction of soluble proteins in lens fiber cells. Similar to the

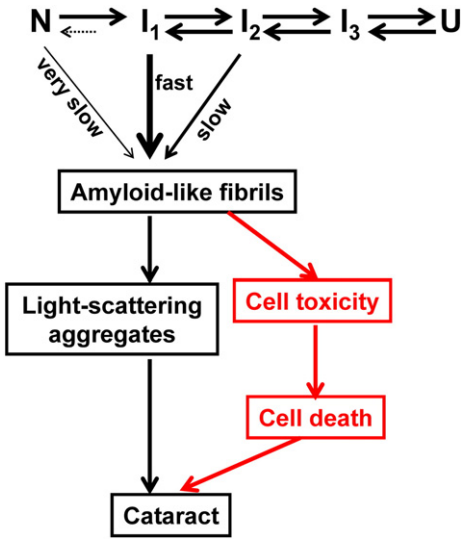

Scheme 1. A proposed model for congenital cataract caused by the G129C mutation in γC-crystallin.

proteins associated with neurodegenerative diseases, crystallins are also able to form amyloid-like fibrils when treated by acidic conditions or low concentrations of denaturants [27–33]. The pathological role of crystallin fibrillization has been hypothesized as initiation of protein aggregation and cataract [3]. In this study, we showed that the G129C mutation greatly promoted the fibrillization/aggregation of γC-crystallin. More importantly, we showed that both the amyloid-like fibrils/aggregates preformed *in vitro* and aggresomes/inclusion bodies formed in the cells exhibited high toxicity to HeLa cell survival and growth. Thus, besides the direct effect of abnormal light scattering, the toxic effect of crystallin fibrils/aggregates might also contribute to the onset of cataract (Scheme 1). Notably, the exogenous expression of the G129C human γC-crystallin in zebrafish embryos results in incomplete lens fiber cell denucleation and the formation of vacuole-like structures in the lens [34]. Similarly, defects in denucleation and lens morphology have also been observed in some of the cataractous mouse models with either overexpression of cataract-causing mutations or knockout of crystallin genes [57–61]. The toxic effects of the aggregated crystallins have a high possibility to hinder lens development by inhibition of lens fiber cell proliferation/maturation and induction of abnormal cell death. Consequently, some of the mutations occurred in lens structural proteins have been associated with non-lens syndrome in the eyes [62], which is not caused by the light scattering of the aggregates but is more likely by the toxic effect of the aggregates. Further *in vivo* research is needed to elucidate the linkage between the toxicity of crystallin aggregates and the phenotypes of both cataract and non-lens syndromes.

Materials and Methods

Materials

Ultra-pure GdnHCl, dithiothreitol, isopropyl-1-thio-β-D-galactopyranoside, ANS, sodium dodecyl sulfate, ThT, bovine serum albumin and antibodies against Flag and β-actin were Sigma products. Plasmid Maxipre kit (#N001) and Vigofect were obtained from Vigorous Biotechnology. Lipofectamine 2000, Hoechst 33342 and other cell culture materials were purchased from Invitrogen. The cell counting kit CCK-8 was from Beyotime. All the other chemicals were local products of analytical grade.

Protein expression and purification

The genes of the WT *CRYAA*, WT *CRYGC* and the G129C mutant of *CRYGC* were obtained as those described previously [34,63]. The genes were cloned to the pET28a plasmids and a six-His tag sequence was fused to the N-terminus of γC-crystallins to facilitate further purification by Ni^{2+} column. αA-Crystallin was constructed without any fusion tag to ensure the correct assembly of αA-crystallin oligomers. The recombinant pET28a plasmids containing the WT or mutated genes were transformed into *Escherichia coli* Rosetta (DE3) for the production of recombinant proteins. Details regarding protein expression and purification of γC-crystallins were the same as those described elsewhere [34] with some modifications. In brief, the *E. coli* cells were grown in the Luria-Bertani medium for 3 h at 37 °C to reach an OD_{400} value of 0.6. Overexpression of the recombinant proteins was induced by the addition of 1 mM isopropyl-1-thio-β-D-galactopyranoside,. After induction, the *E. coli* cells were grown in the Luria-Bertani medium for 20 h at 16 °C. Then the cells were harvested and sonicated by ultrasonic, and the soluble fractions were separated by centrifugation at 12,800*g* at 4 °C. The His-tagged γC-crystallin recombinant proteins in the soluble fractions were collected using a Ni-NTA affinity column and were further purified by a Hiload 16/60 Superdex 200 column equipped on an ÄKTA purifier. The non-tagged αA-crystallin proteins were purified as described previously [64]. The protein solutions were prepared in phosphate-buffered saline (PBS) containing 20 mM sodium phosphate (pH 7.0), 150 mM NaCl, 0.5 mM ethylenediaminetetraacetic acid and 0.5 mM dithiothreitol. The protein concentration was determined by the Bradford method using bovine serum albumin as a standard [65].

Spectroscopy

All spectroscopic experiments were conducted using the same methods as those described elsewhere [22]. In brief, the far-UV CD was measured using a Jasco J-715 spectropolarimeter (Jasco Corp., Tokyo, Japan) with a protein concentration of 0.2 mg/ml. The fluorescence spectra were recorded on an F-2500 fluorescence spectrophotometer (Hitachi Ltd., Tokyo, Japan) with a slit width of 5 nm and a protein concentration was 0.2 mg/ml. The excitation wavelengths of the intrinsic Trp, extrinsic ANS and extrinsic ThT fluorescence were 295 nm, 380 nm

and 440 nm, respectively. The changes in Trp fluorescence spectra were analyzed by monitoring the maximum emission wavelength (E_{max}) and Parameter *A*. Parameter *A*, a sensitive monitor of the position and shape of the Trp fluorescence spectra [66], was calculated by dividing the fluorescence intensity at 320 nm by that at 365 nm (I_{320}/I_{365}). The phase diagram of Trp fluorescence spectra was constructed by plotting I_{320} *versus* I_{365} as described previously [40]. Solution turbidity was detected by the absorbance at 400 nm using an Ultraspec 4300 pro UV/visible spectrophotometer (Amersham Pharmacia Biotech, Uppsala, Sweden).

Protein denaturation induced by GdnHCl

The equilibrium unfolding of the WT and mutated γC-crystallins was performed by denaturing 0.2 mg/ml proteins in PBS containing various concentrations of GdnHCl ranging from 0 to 6 M overnight at 25 °C. The denatured proteins were used for the measurements of far-UV CD, turbidity, intrinsic Trp, extrinsic ANS and extrinsic ThT fluorescence to monitor the structural changes and appearance of aggregates/fibrils during denaturation. The transition curves of the WT protein were fitted by a three-state model using non-linear least-squares regression analysis by Prism 5.0 (GraphPad Inc.).

Protein thermal denaturation

Thermal aggregation kinetics was measured by heating the protein solutions at 70 °C continuously and recording the turbidity data every 2 s. The aggregation kinetics was analyzed by fitting the turbidity data by the following equation [67]:

$$A = A_{lim}(1-\exp(-k(t-t_0)) \quad (1)$$

where *t* is the time of incubation, *A* is the A_{400} value recorded at time *t*, A_{lim} is the A_{400} value at the infinite time, t_0 is the lag time and *k* is the rate constant of aggregation. Data fitting was performed by non-linear regression analysis using the software Prism 5.0 (GraphPad Inc.).

Aggregation during kinetic refolding

The fully denatured proteins were prepared by incubating the proteins in PBS containing 6 M GdnHCl overnight at ambient temperature. Protein aggregation during kinetic refolding was monitored by turbidity every 2 s at 25 °C after the initiation of kinetic refolding by a 1:40 fast manual dilution of the GdnHCl-denatured proteins into the refolding buffer PBS.

Protein fibrillization

The WT and mutated γC-crystallins with a concentration of 5 mg/ml were incubated in PBS containing 0, 0.9 or 1.6 M GdnHCl at 37 °C. The time-course study was performed by measuring the ThT fluorescence and turbidity at different time intervals. The morphology of the aggregates/fibrils was visualized by negatively stained transmission EM. The EM samples were prepared by depositing 0.2 mg/ml protein solutions onto a freshly glow discharged, carbon-coated copper grid, which was negatively stained with 1.25% uranyl acetate for 30 s. The EM experiments were performed on a Hitachi H-7650B microscope with a voltage of 120 kV and a magnification of 68,000×.

MD simulation

Details regarding MD simulation analysis were the same as those described elsewhere [17,34,68]. In brief, the starting structure of the WT human γC-crystallin was constructed by automated protein structure homology modeling provided by SWISS-MODEL [69] using the crystal structures of human γD-crystallin (PDB ID: 1HK0) [42] and mouse γC-crystallin (PDB ID: 2V2U) [43] as modeling templates [34]. The starting structure of the G129C mutant was built using VMD [70] based on the modeled structure of the WT human γC-crystallin. The simulation systems contained a water box, 150 mM NaCl and 0, 0.9 or 1.6 M GdnHCl generated by VMD. Equilibrium simulations were performed using NAMD 2.8 package [71] at 2 fs time steps for 20 ns at 450 K and constant pressure (1 atm). The aggregation tendency of each residue was quantified by calculating SAP [46] values as described previously [68]. The positioning of NTD and CTD of γC-crystallin was estimated by measuring the angle between the axes parallel with the central β-strands of the Greek-key motifs. The interdomain binding energy was calculated by the VMD plugin NAMD energy. The domain interface areas were determined using the online service of PISA (*P*rotein *I*nterfaces, *S*urfaces and *A*ssemblies) algorithm PDBePISA[‡] [45]. The analysis and rendering of the structures were performed using the software PyMOL (The PyMOL Molecular Graphics System, Version 0.99rc6, Schrödinger, LLC[§]).

Cell culture and immunofluorescence

The HeLa cells were obtained from the China center of American Type Culture Collection. The cells were cultured in Dulbecco's modified Eagle's medium (DMEM; Gibco) containing 10% fetal bovine serum at 37 °C in 5% CO_2 incubator. The genes of the WT and mutated *CRYGC* were inserted into the eukaryotic expression vector pEGFP-N1 or pCDNA 3.1 N-Flag. The HeLa cells were seeded on glass coverslides treated with 2.5 M NaOH and 60% ethanol. After cultivation for 24 h to reach 90% confluency, the cells were transiently transfected with plasmids containing the WT or mutated *CRYGC* genes using Lipofectamine 2000 (Invitrogen) following the instructions of the manufacturer. After transfection for 4 h, the cells were cultivated in fresh DMEM high-glucose medium to remove the transfection reagent and residual plasmids. After 24 h of cultivation, the transfected cells were fixed by 4% paraformaldehyde for 40 min and washed by PBS for three times. Immunostaining was achieved by mouse anti-p62 antibody (Abcam, 1:200) in PBS containing 5% normal goat serum and incubated for 1 h at 37 °C, followed by incubating with Alexa-649-conjugated goat anti-mouse IgG (1:250) for 1 h at room temperature. The nuclei were counterstained with Hoechst 33342. The mounted cells were visualized using a Carl Zeiss LSM 710 confocal microscope.

Cell viability assay

The effect of the G129C mutant on cell viability was measured using CCK-8 (Beyotime, China) according to the manufacturer's instructions. The HeLa cells were seeded in 96-well culture plates with 1000 cells in each well and cultured in DMEM medium. Cell viability was evaluated by treating the cells with preformed aggregates from the recombinant proteins. The preformed aggregates were obtained by incubating 5 mg/ml WT or mutated γC-crystallin protein in PBS containing 0, 0.9 or 1.6 M GdnHCl at 37 °C for 72 h. The cells were treated with the preformed aggregates with a protein concentration of 40 μg/ml (2 μM) or 4 μg/ml (0.2 μM) for 48 h. The cells treated with the same buffer without proteins were used as the control. After treatment, each well of cells was added with 10 μl of CCK-8 reagent and incubated at 37 °C for 1 h. Then the absorbance at 450 nm was measured using a microplate reader (Bio-Rad Model-680). Cell viability was calculated by dividing the absorbance of the treated group by that of the control group. All viability experiments were repeated at least three times.

Cell growth assay

The overexpression of the WT or mutated γC-crystallin was achieved by transient transfection of the HeLa cells with plasmids containing *Flag-CRYGC*. The cells transfected with pCDNA 3.1 N-Flag were used as the control. The transfected cells were cultivated with different time intervals. The expression level of the WT or mutated γC-crystallin was evaluated by Western blot analysis using anti-Flag and anti-actin antibodies. β-Actin was used as the protein loading control for the Western blot analysis. After cultivation, the cells was treated with the CCK-8 reagent and incubated at 37 °C for 1 h. Then the absorbance at 450 nm was recorded using a microplate reader (Bio-Rad Model-680).

Cell apoptosis assay

The HeLa cells were transfected with the WT or mutated *CRYGC* genes. After transfection for 4 h, the cultivation medium was refreshed to remove the transfection reagent and cultivated for another 24 h. Then the cells were harvested, washed by PBS for three times and resuspended in annexin V binding buffer. The cells were stained with PI and FITC-labeled annexin V (BD Biosciences) according to the manufacturer's instructions. Apoptosis analysis was determined by separating the PI- and/or FITC-positive cells using FITC Annexin V Apoptosis Detection Kit 1 (BD Pharmingen 556547) on a FACSCalibur flow cytometer (BD Biosciences). The ratio of death cells was calculated from three independent experiments.

Acknowledgements

The authors thank H. Gong and H. Liu for suggestions with MD simulations; Y. Li for help with EM measurements; H.-C. Cai, F.-C. Bao and S. Wang for help and suggestions with the folding experiments; and S. Wang for help with proofreading.

Author Contributions: Y.-B.Y. conceived and designed the experiments. Y.-B.X., X.-J.C. and W.-J.Z. performed the experiments. Y.-B.X., X.-J.C., W.-J.Z. and Y.-B.Y. analyzed the data. Y.-B.Y. wrote the paper.

Funding: This study was supported by funds from the Ministry of Science and Technology of China (2012BAI08B01) and State Key Laboratory of Membrane Biology.

Appendix A. Supplementary data

Supplementary data to this article can be found online at http://dx.doi.org/10.1016/j.jmb.2015.07.001.

Received 11 February 2015;
Received in revised form 18 June 2015;
Accepted 1 July 2015
Available online 9 July 2015

Keywords:
γC-crystallin;
disease-causing mutation;
autosomal dominant congenital nuclear cataract;
aggregation-prone unfolding intermediate;
cell toxicity

† Y.-B.X., X.-J.C. and W.-J.Z. contributed equally to this work.
‡ http://www.ebi.ac.uk/pdbe/prot_int/pistart.html
§ http://www.pymol.org/

Abbreviations used:
ANS, 1-anilinonaphthalene-8-sulfonate; CTD, C-terminal domain; DMEM, Dulbecco's modified Eagle's medium; EM, electron microscope; GdnHCl, guanidine hydrochloride; MD, molecular dynamics; NTD, N-terminal domain; PBS, phosphate-buffered saline; PI, propidium iodide; SAP, spatial aggregation propensity; ThT, thioflavin T; WT, wild type.

References

[1] C.M. Dobson, Protein folding and misfolding, Nature 426 (2003) 884–890.
[2] F. Chiti, C.M. Dobson, Protein misfolding, functional amyloid, and human disease, Annu. Rev. Biochem. 75 (2006) 333–366.
[3] K.L. Moreau, J.A. King, Protein misfolding and aggregation in cataract disease and prospects for prevention, Trends Mol. Med. 18 (2012) 273–282.
[4] S. Seshadri, K.A. Oberg, V.N. Uversky, Mechanisms and consequences of protein aggregation: the role of folding intermediates, Curr. Protein Pept. Sci. 10 (2009) 456–463.

[5] V.N. Uversky, A.L. Fink, Conformational constraints for amyloid fibrillation: the importance of being unfolded, Biochim. Biophys. Acta 1698 (2004) 131–153.
[6] E.M. Sontag, W.I. Vonk, J. Frydman, Sorting out the trash: the spatial nature of eukaryotic protein quality control, Curr. Opin. Cell Biol. 26 (2014) 139–146.
[7] S. Wickner, M. Maurizi, S. Gottesman, Posttranslational quality control: folding, refolding, and degrading proteins, Science 286 (1999) 1888–1893.
[8] L. Robman, H. Taylor, External factors in the development of cataract, Eye (London) 19 (2005) 1074–1082.
[9] C.J. Hammond, H. Snieder, T.D. Spector, C.E. Gilbert, Genetic and environmental factors in age-related nuclear cataracts in monozygotic and dizygotic twins, N. Engl. J. Med. 342 (2000) 1786–1790.
[10] A. Shiels, J.F. Hejtmancik, Genetics of human cataract, Clin. Genet. 84 (2013) 120–127.
[11] H. Bloemendal, W. de Jong, R. Jaenicke, N.H. Lubsen, C. Slingsby, A. Tardieu, Ageing and vision: structure, stability and function of lens crystallins, Prog. Biophys. Mol. Biol. 86 (2004) 407–485.
[12] G.B. Benedek, Cataract as a protein condensation disease: the proctor lecture, Invest. Ophthalmol. Vis. Sci. 38 (1997) 1911–1921.
[13] V. Talla, N. Srinivasan, D. Balasubramanian, Visualization of in situ intracellular aggregation of two cataract-associated human γ-crystallin mutants: lose a tail, lose transparency, Invest. Ophthalmol. Vis. Sci. 49 (2008) 3483–3490.
[14] K.O. Muranov, O.I. Maloletkina, N.B. Poliansky, K.A. Markossian, S.Y. Kleymenov, S.P. Rozhkov, et al., Mechanism of aggregation of UV-irradiated β_L-crystallin, Exp. Eye Res. 92 (2011) 76–86.
[15] S.G. Roman, N.A. Chebotareva, T.B. Eronina, S.Y. Kleymenov, V.F. Makeeva, N.B. Poliansky, et al., Does the crowded cell-like environment reduce the chaperone-like activity of α-crystallin? Biochemistry 50 (2011) 10607–10623.
[16] V.P.R. Vendra, G. Agarwal, S. Chandani, V. Talla, N. Srinivasan, D. Balasubramanian, Structural integrity of the Greek key motif in βγ-crystallins is vital for central eye lens transparency, PLoS ONE 8 (2013) e70336.
[17] S. Wang, W.J. Zhao, H. Liu, H. Gong, Y.B. Yan, Increasing βB1-crystallin sensitivity to proteolysis caused by the congenital cataract-microcornea syndrome mutation S129R, Biochim. Biophys. Acta 1832 (2013) 302–311.
[18] Z. Xia, Z. Yang, T. Huynh, J.A. King, R. Zhou, UV-radiation induced disruption of dry-cavities in human γD-crystallin results in decreased stability and faster unfolding, Sci. Rep. 3 (2013) 1560.
[19] J.I. Clark, Self-assembly of protein aggregates in ageing disorders: the lens and cataract model, Philos. Trans. R. Soc. Lond. B Biol. Sci. 368 (2013) 20120104.
[20] Y. Chen, D.C. Thompson, V. Koppaka, J.V. Jester, V. Vasiliou, Ocular aldehyde dehydrogenases: protection against ultraviolet damage and maintenance of transparency for vision, Prog. Retin. Eye Res. 33 (2013) 28–39.
[21] K. Zhang, W.J. Zhao, X.Y. Leng, S. Wang, K. Yao, Y.B. Yan, The importance of the last strand at the C-terminus in βB2-crystallin stability and assembly, Biochim. Biophys. Acta 1842 (2014) 44–55.
[22] Y.B. Xi, W.J. Zhao, X.T. Zuo, H.C. Tjondro, J. Li, A.B. Dai, et al., Cataract-causing mutation R233H affects the stabilities of βB1- and βA3/βB1-crystallins with different pH-dependence, Biochim. Biophys. Acta 1842 (2014) 2216–2229.
[23] U.P. Andley, Crystallins in the eye: function and pathology, Prog. Retin. Eye Res. 26 (2007) 78–98.
[24] P. Chen, W. Ji, F.Y. Liu, H.Z. Tang, S. Fu, X. Zhang, et al., Alpha-crystallins and tumorigenesis, Curr. Mol. Med. 12 (2012) 1164–1173.
[25] R. Kannan, P.G. Sreekumar, D.R. Hinton, Novel roles for α-crystallins in retinal function and disease, Prog. Retin. Eye Res. 31 (2012) 576–604.
[26] J.S. Zigler, C. Zhang, R. Grebe, G. Sehrawat, L. Hackler, S. Adhya, et al., Mutation in the βA3/A1-crystallin gene impairs phagosome degradation in the retinal pigmented epithelium of the rat, J. Cell Sci. 124 (2011) 523–531.
[27] S. Meehan, Y. Berry, B. Luisi, C.M. Dobson, J.A. Carver, C.E. MacPhee, Amyloid fibril formation by lens crystallin proteins and its implications for cataract formation, J. Biol. Chem. 279 (2004) 3413–3419.
[28] S. Meehan, T.P.J. Knowles, A.J. Baldwin, J.F. Smith, A.M. Squires, P. Clements, et al., Characterisation of amyloid fibril formation by small heat-shock chaperone proteins human αA-, αB- and R120G αB-crystallins, J. Mol. Biol. 372 (2007) 470–484.
[29] K. Papanikolopoulou, I. Mills-Henry, S.L. Thol, Y. Wang, A.A. Gross, D.A. Kirschner, et al., Formation of amyloid fibrils *in vitro* by human γD-crystallin and its isolated domains, Mol. Vis. 14 (2008) 81–89.
[30] H. Ecroyd, J.A. Carver, Crystallin proteins and amyloid fibrils, Cell. Mol. Life Sci. 66 (2009) 62–81.
[31] Y. Wang, S. Petty, A. Trojanowski, K. Knee, D. Goulet, I. Mukerji, et al., Formation of amyloid fibrils *in vitro* from partially unfolded intermediates of human γC-crystallin, Invest. Ophthalmol. Vis. Sci. 51 (2010) 672–678.
[32] S.D. Moran, A.M. Woys, L.E. Buchanan, E. Bixby, S.M. Decatur, M.T. Zanni, Two-dimensional IR spectroscopy and segmental ^{13}C labeling reveals the domain structure of human γD-crystallin amyloid fibrils, Proc. Natl. Acad. Sci. U. S. A. 109 (2012) 3329–3334.
[33] Y.B. Xi, K. Zhang, A.B. Dai, S.R. Ji, K. Yao, Y.B. Yan, Cataract-linked mutation R188H promotes βB2-crystallin aggregation and fibrillization during acid denaturation, Biochem. Biophys. Res. Commun. 447 (2014) 244–249.
[34] X.Q. Li, H.C. Cai, S.Y. Zhou, J.H. Yang, Y.B. Xi, X.B. Gao, et al., A novel mutation impairing the tertiary structure and stability of γC-crystallin (*CRYGC*) leads to cataract formation in humans and zebrafish lens, Hum. Mutat. 33 (2012) 391–401.
[35] L. Fu, J.J. Liang, Unfolding of human lens recombinant βB2- and γC-crystallins, J. Struct. Biol. 139 (2002) 191–198.
[36] L. Fu, J.J. Liang, Spectroscopic analysis of lens recombinant βB2- and γC-crystallin, Mol. Vis. 7 (2001) 178–183.
[37] M.S. Kosinski-Collins, S.L. Flaugh, J. King, Probing folding and fluorescence quenching in human γD crystallin Greek key domains using triple tryptophan mutant proteins, Protein Sci. 13 (2004) 2223–2235.
[38] M.S. Kosinski-Collins, J. King, *In vitro* unfolding, refolding, and polymerization of human γD crystallin, a protein involved in cataract formation, Protein Sci. 12 (2003) 480–490.
[39] S. Wang, X.Y. Leng, Y.B. Yan, The benefits of being β-crystallin heteromers: βB1-crystallin protects βA3-crystallin against aggregation during co-refolding, Biochemistry 50 (2011) 10451–10461.
[40] N.A. Bushmarina, I.M. Kuznetsova, A.G. Biktashev, K.K. Turoverov, V.N. Uversky, Partially folded conformations in the folding pathway of bovine carbonic anhydrase II: a fluorescence spectroscopic analysis, Chembiochem 2 (2001) 813–821.

[41] S. Mishra, R.A. Stein, H.S. McHaourab, Cataract-linked γD-crystallin mutants have weak affinity to lens chaperones α-crystallins, FEBS Lett. 586 (2012) 330–336.
[42] A. Basak, O. Bateman, C. Slingsby, A. Pande, N. Asherie, O. Ogun, et al., High-resolution X-ray crystal structures of human γD crystallin (1.25 Å) and the R58H mutant (1.15 Å) associated with aculeiform cataract, J. Mol. Biol. 328 (2003) 1137–1147.
[43] A.G. Purkiss, O.A. Bateman, K. Wyatt, P.A. Wilmarth, L.L. David, G.J. Wistow, et al., Biophysical properties of γC-crystallin in human and mouse eye lens: the role of molecular dipoles, J. Mol. Biol. 372 (2007) 205–222.
[44] J. Chen, S.L. Flaugh, P.R. Callis, J. King, Mechanism of the highly efficient quenching of tryptophan fluorescence in human γD-crystallin, Biochemistry 45 (2006) 11552–11563.
[45] E. Krissinel, K. Henrick, Inference of macromolecular assemblies from crystalline state, J. Mol. Biol. 372 (2007) 774–797.
[46] N. Chennamsetty, V. Voynov, V. Kayser, B. Helk, B.L. Trout, Design of therapeutic proteins with enhanced stability, Proc. Natl. Acad. Sci. U. S. A. 106 (2009) 11937–11942.
[47] P. Das, J.A. King, R. Zhou, Aggregation of γ-crystallins associated with human cataracts via domain swapping at the C-terminal β-strands, Proc. Natl. Acad. Sci. U. S. A. 108 (2011) 10514–10519.
[48] J.L. England, V.S. Pande, G. Haran, Chemical denaturants inhibit the onset of dewetting, J. Am. Chem. Soc. 130 (2008) 11854–11855.
[49] M. Perutz, Electrostatic effects in proteins, Science 201 (1978) 1187–1191.
[50] E. Serebryany, J.A. King, The βγ-crystallins: native state stability and pathways to aggregation, Prog. Biophys. Mol. Biol. 115 (2014) 32–41.
[51] M. Stefani, Protein misfolding and aggregation: new examples in medicine and biology of the dark side of the protein world, Biochim. Biophys. Acta 1739 (2004) 5–25.
[52] O.I. Povarova, I.M. Kuznetsova, K.K. Turoverov, Differences in the pathways of proteins unfolding induced by urea and guanidine hydrochloride: molten globule state and aggregates, PLoS One 5 (2010) e15035.
[53] W.D. Brubaker, J.A. Freites, K.J. Golchert, R.A. Shapiro, V. Morikis, D.J. Tobias, et al., Separating instability from aggregation propensity in γS-crystallin variants, Biophys. J. 100 (2011) 498–506.
[54] A.K. Bhuyan, Protein stabilization by urea and guanidine hydrochloride, Biochemistry 41 (2002) 13386–13394.
[55] N. Shukla, A.N. Bhatt, A. Aliverti, G. Zanetti, V. Bhakuni, Guanidinium chloride- and urea-induced unfolding of FprA, a mycobacterium NADPH-ferredoxin reductase Stabilization of an apo-protein by GdmCl, FEBS J. 272 (2005) 2216–2224.
[56] R.L. Remmele, J. Zhang-van Enk, D. Phan, L. Yu, Stabilization by urea during thermal unfolding-mediated aggregation of recombinant human interleukin-1 receptor (type II): does solvation entropy play a role? J. Phys. Chem. B 116 (2012) 7240–7251.
[57] Z. Ma, W. Yao, V. Theendakara, C.C. Chan, E. Wawrousek, J.F. Hejtmancik, Overexpression of human γC-crystallin 5 bp duplication disrupts lens morphology in transgenic mice, Invest. Ophthalmol. Vis. Sci. 52 (2011) 5369–5375.
[58] U.P. Andley, αA-crystallin R49C^{neo} mutation influences the architecture of lens fiber cell membranes and causes posterior and nuclear cataracts in mice, BMC Ophthalmol. 9 (2009) 4.
[59] J. Graw, A. Neuhauser-Klaus, N. Klopp, P.B. Selby, J. Loster, J. Favor, Genetic and allelic heterogeneity of *Cryg* mutations in eight distinct forms of dominant cataract in the mouse, Invest. Ophthalmol. Vis. Sci. 45 (2004) 1202–1213.
[60] S.K. Brahma, S. Sanyal, Immunohistochemical studies of lens crystallins in the dysgenetic lens (*dyl*) mutant mice, Exp. Eye Res. 38 (1984) 305–311.
[61] K. Wang, C. Cheng, L. Li, H. Liu, Q. Huang, C.H. Xia, et al., γD-crystallin associated protein aggregation and lens fiber cell denucleation, Invest. Ophthalmol. Vis. Sci. 48 (2007) 3719–3728.
[62] A. Churchill, J. Graw, Clinical and experimental advances in congenital and paediatric cataracts, Philos. Trans. R. Soc. Lond. B Biol. Sci. 366 (2011) 1234–1249.
[63] F. Gu, W. Luo, X. Li, Z. Wang, S. Lu, M. Zhang, et al., A novel mutation in αA-crystallin (*CRYAA*) caused autosomal dominant congenital cataract in a large Chinese family, Hum. Mutat. 29 (2008) 769.
[64] T.-X. Sun, B.K. Das, J.J.N. Liang, Conformational and functional differences between recombinant human lens αA- and αB-crystallin, J. Biol. Chem. 272 (1997) 6220–6225.
[65] M.M. Bradford, A rapid and sensitive method for the quantitation of microgram quantities of protein utilizing the principle of protein-dye binding, Anal. Biochem. 72 (1976) 248–254.
[66] K.K. Turoverov, S.Y. Haitlina, G.P. Pinaev, Ultra-violet fluorescence of actin. Determination of native actin content in actin preparations, FEBS Lett. 62 (1976) 4–6.
[67] B.I. Kurganov, Kinetics of protein aggregation. Quantitative estimation of the chaperone-like activity in test-systems based on suppression of protein aggregation, Biochemistry (Moscow) 67 (2002) 409–422.
[68] Z. Chen, X.-J. Chen, M. Xia, H.-W. He, S. Wang, H. Liu, et al., Chaperone-like effect of the linker on the isolated C-terminal domain of rabbit muscle creatine kinase, Biophys. J. 103 (2012) 558–566.
[69] K. Arnold, L. Bordoli, J. Kopp, T. Schwede, The SWISS-MODEL workspace: a Web-based environment for protein structure homology modelling, Bioinformatics 22 (2006) 195–201.
[70] W. Humphrey, A. Dalke, K. Schulten, VMD: visual molecular dynamics, J. Mol. Graph. 14 (1996) 27–28.
[71] J.C. Phillips, R. Braun, W. Wang, J. Gumbart, E. Tajkhorshid, E. Villa, et al., Scalable molecular dynamics with NAMD, J. Comput. Chem. 26 (2005) 1781–1802.